HHS Public Access

Author manuscript

J Control Release. Author manuscript; available in PMC 2019 August 10.

Published in final edited form as:

J Control Release. 2018 August 10; 283: 94–104. doi:10.1016/j.jconrel.2018.05.014.

Intra-vitreal αB crystallin fused to elastin-like polypeptide provides neuroprotection in a mouse model of age-related macular degeneration

Parameswaran G. Sreekumar[#a], **Zhe Li**[#b], **Wan Wang**[b], **Christine Spee**[c], **David R. Hinton**[c,d,2], **Ram Kannan**[a,2], and **J. Andrew MacKay**[b,c,e,*,2]

[a]Arnold and Mabel Beckman Macular Research Center, Doheny Eye Institute, Los Angeles, CA 90033, USA

[b]Department of Pharmacology and Pharmaceutical Sciences, School of Pharmacy of the University of Southern California, Los Angeles, CA 90089, USA

[c]Department Ophthalmology, USC Roski Eye Institute, Keck School of Medicine of the University of Southern California, Los Angeles, CA 90033, USA

[d]Department of Pathology, Keck School of Medicine of the University of Southern California, Los Angeles, CA 90033, USA

[e]Department of Biomedical Engineering, Viterbi School of Engineering of the University of Southern California, Los Angeles, CA 90033, USA

[#] These authors contributed equally to this work.

Abstract

Age-related macular degeneration (AMD) is the leading cause of severe and irreversible central vision loss, and the primary site of AMD pathology is the retinal pigment epithelium (RPE). Geographic atrophy (GA) is an advanced form of AMD characterized by extensive RPE cell loss, subsequent degeneration of photoreceptors, and thinning of retina. This report describes the protective potential of a peptide derived from the αB crystallin protein using a sodium iodate ($NaIO_3$) induced mouse model of GA. Systemic $NaIO_3$ challenge causes degeneration of the RPE and neighboring photoreceptors, which have similarities to retinas of GA patients. αB crystallin is an abundant ocular protein that maintains ocular clarity and retinal homeostasis, and a small peptide from this protein (mini cry) displays neuroprotective properties. To retain this peptide for longer in the vitreous, mini cry was fused to an elastin-like polypeptide (ELP). A single intra-vitreal treatment by this crySI fusion significantly inhibits retinal degeneration in comparison to free mini cry. While mini cry is cleared from the eye with a mean residence time of 0.4 days, crySI is retained with a mean residence time of 3.0 days; furthermore, fundus photography reveals evidence of retention at two weeks. Unlike the free mini cry, crySI protects the RPE against $NaIO_3$

[*]Corresponding author at: Department of Pharmacology and Pharmaceutical Sciences, School of Pharmacy, University of Southern California, 1985 Zonal Ave, Los Angeles, CA, 90089, USA. jamackay@usc.edu (J.A. MacKay).

[2]Co-senior authors.

Appendix A. Supplementary data

Supplementary data to this article can be found online at https://doi.org/10.1016/j.jconrel.2018.05.014.

challenge for at least two weeks after administration. CrySI also inhibits RPE apoptosis and caspase-3 activation and protects the retina from cell death up to 1-month post $NaIO_3$ challenge. These results show that intra-ocular ELP-linked peptides such as crySI hold promise as protective agents to prevent RPE atrophy and progressive retinal degeneration in AMD.

Keywords

Elastin-like polypeptides; Geographic atrophy; αB crystalline; RPE cell death; Retinal degeneration; $NaIO_3$

1. Introduction

Age-related macular degeneration (AMD), the leading cause of irreversible visual loss in the elderly, is complicated by two blinding late forms of the disease: choroidal neovascularization (CNV) and geographic atrophy (GA) or atrophic AMD. GA is an advanced form of dry AMD with extensive atrophy and loss of the retinal pigment epithelium (RPE) and overlying photoreceptors and is responsible for 10–20% of cases of legal blindness from AMD [1,2]. There are effective treatments for complications developing from neovascular AMD, but there is neither a treatment of the atrophic form of AMD nor effective preventive strategies against progression to the neovascular form of AMD [3]. Therefore, development of effective protective drugs against atrophic AMD is greatly needed.

Intra-venous injection of sodium iodate ($NaIO_3$), a stable oxidizing agent, specifically damages the RPE layer resulting in secondary retinal degeneration recapitulating some of the morphological features seen in GA [4–6]. The $NaIO_3$ mouse model has been well characterized with respect to the loss of RPE cells and the death of photoreceptors, resulting in a thinning of the outer nuclear layer (ONL) and a reduction in visual functions [5–7]. $NaIO_3$ retinal toxicity has been demonstrated in many different mammalian species, including sheep [8], rabbit [9], rat [10], and mouse [6,11]. Currently systemic administration of $NaIO_3$ has been extensively used as a pre-clinical model of RPE dystrophy and atrophic forms of AMD. It is of interest that a recent study suggests that prolonged exposure to non-lethal doses of $NaIO_3$ retard cell migration, decrease vascular endothelial growth factor (VEGF) levels, and attenuate phagocytic activity of RPE cells [12]. Using a model of retinal degeneration induced by a single challenge of $NaIO_3$, this study explores the protective effect of a fragment of the αB crystallin protein.

Within the family of small heat shock proteins, the α-crystallins possess multiple functions [13]. Among the α-crystallins, αB crystallin is highly expressed in RPE cells [14]. αB crystallin acts as a molecular chaperone, preventing aggregation of proteins and inhibiting oxidative stress-induced cell death and disruption of cytoskeletal assembly. It also inhibits inflammation and provides neuroprotection [13]. Exogenous administration of full length αB crystallin to mice ameliorates neuroinflammation [15,16], autoimmune encephalomyelitis [17], optic neuropathy [18], ischemia-reperfusion injury [19], stroke [20], and acute spinal cord injury [21]. The fundamental properties of several individual peptides of α-crystallin have been the extensive work of the laboratories of Sharma [22,23] and Clark

[24–26]. These studies reveal that short peptide fragments from the intact protein have anti-apoptotic activity and several binding partners [26]. In particular, a 20-mer peptide (mini cry) derived from the amino acid residues 73–92 of αB crystallin protects RPE cells from oxidative stress induced cell death by inhibiting caspase-3 activation [27]. Kurnellas et al. showed that mini cry binds inflammatory mediators in plasma thereby reducing paralysis in experimental autoimmune encephalomyelitis [28]. Compared to the full-length protein, the mini cry peptide not only maintains its bioactivity but also offers advantages including the relative ease of crossing tissue barriers, providing active doses, lower production complexity and less side effects [29]. An intrinsic weakness, however, of using low molecular weight peptides is that they tend to be cleared rapidly from the ocular compartments, demanding repeated injections which could have serious complications such as vitreous hemorrhage, and retinal detachment [30,31].

To avoid difficulties encountered with intra-ocular delivery and rapid turnover of low molecular weight peptides [32–34], in our previous study mini cry was recombinantly fused with a high molecular weight elastin-like polypeptide (ELP) called SI, which assembles multivalent nanoparticles at physiological temperature [35]. ELPs are biopolymers derived from a structural motif found in the mammalian tropoelastin protein, which phase separate above tunable transition temperatures. Below this temperature they maintain high solubility and tissue permeability. Above the transition temperature, they form a viscous secondary aqueous phase that can enhance tissue retention [36,37]. ELPs are genetically encoded; therefore, their DNA coding sequence was first modified to also encode residues 73–92 of the αB crystallin sequence. Thus, a genetically modified cytoprotective polypeptide composed of ELP, and the mini cry peptide (crySI) was expressed and purified from *Escherichia coli*. Our earlier work established that crySI ELPs have chaperone activity, enter human RPE cells and protect them from oxidative stress induced cell death by inhibiting caspase-3 activation [35]. However, the protective potential of crySI in animal models of AMD has not been established so far.

The hypothesis examined by the present study is that sustained local availability of crySI prevents RPE death and rescues photoreceptors in a $NaIO_3$ – challenged retinal degeneration mouse model to a greater extent than for free mini cry. To examine the validity of this drug-delivery strategy, the effect of crySI on the severity of retinal degeneration were tracked by ocular pharmacokinetics, fundus photography, retinal histology, retention of labeled peptides, markers of cell death, and evaluation with a primary human RPE polarized monolayer.

2. Materials and methods

2.1. Materials and reagents

Mini cry (NH2-DRFSVNLDVKHFSPEELKVK-COOH, M.W. = 2.388 kD, 98.1% purity) and fluorescein-labeled mini cry (NH2-DRFSVNLDVKHFSPEELKVK(FITC)-COOH, M.W. = 2.777 kD, 98.6% purity) were chemically synthesized by Neo-peptide (Cambridge, MA). Purified ELP was labeled with NHS-fluorescein (#46410, ThermoFisher Scientific Inc., Rockford, IL). An antibody that recognizes cleaved caspase-3 (#9661) was purchased from Cell Signaling Tech (Boston, MA) and a fluorescein goat anti-rabbit secondary

antibody was purchased from Vector Laboratory (Burlingame, CA). *In situ* Cell Death Detection Kit (#12156792910), TMR red was purchased from Roche (Roche Applied Science, IN). Rabbit αB crystallin antibodies (#ADI-SPA-223) were procured from Enzo Life Sciences (Farmingdale, NY). FITC- anti-mouse CD3 antibody was obtained from BioLegend (# 100203, San Diego, CA).

2.2. ELP expression and purification

ELPs were expressed in BLR (DE3) *Escherichia coli* chemically competent cells (Novagen Inc., Milwaukee, WI) and purified *via* inverse transition cycling (ITC) as previously reported [35]. Purity was assessed by running 10 μg of polymer on a 4–20% SDS-PAGE gel stained with 10% copper chloride. Unlabeled ELP concentrations were determined by UV–Visible spectroscopy at 280 nm E_{ELP} = 1285 M^{-1} cm^{-1}). For preparations intended for *in vivo* evaluation, additional removal of endotoxin was required. Detoxi-gel chromatography (ThermoFisher Scientific Inc., Rockford, IL) was used to reduce endotoxin on a small scale for volumes of 0.5 mL, and the Mustang Acrodisc syringe filter (Pall Corporation, Port Washington, NY) were used to clear protein samples on a larger scale of volumes of 10 mL. Endotoxin burden was estimated using a Pryogent Gel Clot assay (N289–06, Lonza, Walkersville, MD). The endotoxin level of SI and crySI injected into the mouse vitreous was confirmed to be lower than 60 EU/mL (lower than 0.1 EU/eye) based on a negative test result for a 1:1000 dilution into PBS (sensitivity = 0.06 EU/mL).

2.3. Fluorescent labeling of ELPs

For fluorescent visualization, SI (control ELP) and crySI were covalently modified with NHS-Fluorescein (Thermo Fisher Scientific Inc., Rockford, IL) by conjugation to free amines. Briefly, crySI was mixed with a 3-fold molar excess of NHS-Fluorescein in phosphate buffered saline (PBS) and incubated at 4 °C for 3 h. Free fluorophore was removed by size exclusion chromatography using a Zeba desalt spin column (89891, Thermo Fisher Scientific Inc., Rockford, IL). The concentration of label after the purification, $C_{FL\text{-}crySI}$, was estimated as follows:

$$C_{FL-crySI} = \frac{A_{493\ nm}}{\varepsilon_{fluor}} \quad (1)$$

where the molar extinction coefficient of fluorescein, E_{fluor}, was assumed to be 70,000 M^{-1} cm^{-1}. Due to the low molar extinction coefficient of the crySI relative to the contribution of fluorescein at an optical absorbance of 280 nm, the degree of labeling, $N_{labeling}$, was estimated as follows:

$$N_{labeling} = \frac{n_{FL-crySI,purified}}{n_{crySI,reacted}} \quad (2)$$

where $n_{crySI,reacted}$ and $n_{FL\text{-}crySI,purifled}$ are the moles of crySI reacted and fluorescein recovered after purification respectively. Fluorescein labeled FL-crySI had a labeling

efficiency ~0.6. To determine the purity of labeled materials, proteins were separated on SDS-PAGE gels and imaged on a ChemiDoc Touch Imaging System (Bio-Rad Laboratories, Hercules, CA).

2.4. $NaIO_3$-induced geographic atrophy mouse model

The 129S6/SvEvTac wild type male mice were purchased from Taconic Farms (Germantown, NY). Mice aged between 4 and 8 weeks maintained on a standard laboratory chow in an air-conditioned room equipped with a 12-hour light/12-hour dark cycle were used in all studies. All animal procedures conformed to the guidelines on the Use of Animals from the NIH and the Association for Research in Vision and Ophthalmology (ARVO) and were approved by the University of Southern California Institutional Animal Care and Use Committee. The $NaIO_3$-induced mouse model of acute RPE atrophy has been well characterized in our laboratory [6]. Prior to challenge, intra-vitreal injections (2 μE) in mice were performed using a Hamilton 32 gauge needle (Hamilton, Reno, NV). Male mice (4–8 weeks old) were randomly divided into two groups (n = 10). In the first group, the right and left eyes received intra-vitreal injection of crySI (250 μM) and SI (250 μM), respectively. In the second group; mini cry alone was injected to the right eye while the left eye received PBS. Following intra-vitreal administration by 2, 7, or 14 days a single intra-venous (tail vein) injection of sterile $NaIO_3$ (Sigma-Aldrich, USA) was administered in phosphate-buffered saline (PBS) at a challenge of 33 mg/kg body-weight. For mice treated 2 days prior to $NaIO_3$ challenge, color fundus images were obtained after one week and retinas were processed for histology, TUNEL staining, and immunofluorescent microscopy. For mice treated 7 and 14 days prior to $NaIO_3$ challenge, color fundus images and retinas were obtained after one month to assess long-term effects. Areas of retinal degeneration were quantified using ImageJ (US NIH, Bethesda, MD).

2.5. Color fundus photography

Mice were anesthetized by administration of ketamine and xylazine. For all animals, pupils were dilated with one to two drops of Tropicamide Ophthalmic Solution 1% (Bausch & Lomb, Tampa, FL) 5 min prior to imaging. A hydroxypropyl methylcellulose ophthalmic demulcent solution (Gonak, Akorn Lake Forest, IL) was applied to the eye to provide a uniform optically transparent interface between the tip of the endoscope and the cornea of the subject. Images were captured using a 35 mm Kowa hand-held color fundus camera (Genesis, Tokyo, Japan). 4–6 images were taken from each eye.

2.6. Quantification of retinal degeneration from fundus imaging

To quantify areas of retinal degeneration, the image was opened with ImageJ (US NIH, Bethesda, MD) and converted to a 16-bit image [38]. The image was then thresholded, the type was set to black & white. The binary image was used to quantify the relative area of degeneration. To calculate the percentage of retinal degeneration, the areas with degeneration and total fundus area were determined from each image. The ratio between the degenerated area and total area was estimated for each eye over time.

2.7. Quantitative analysis of fluorescence in color fundus images

To compare the intra-ocular disposition of SI, crySI and the free mini cry peptide, fluorescein-labeled samples in PBS (2 μE, 70 μM) were injected into the vitreous as described above and observed by color fundus photography using a bright white illumination source. The area specifically emitting a green fluorescent signal was selected by defining the region of interest (ROI). The fluorescent intensities within these regions were analyzed using ImageJ (US NIH, Bethesda, MD). Briefly, captured color images were converted to RGB stacks and the integrated intensity of each channel was measured. To correct the green signal for nonspecific scattering of white light in each image, the intensity of the green channel was corrected for background by the blue channel. From this corrected value, the background signal observed in PBS-treated eyes was subtracted. This background-subtracted intensity was normalized to signal, Fl_{normal}, obtained immediately after the injection of crySI ($t = 0$) as follows:

$$Fl_{normal} = \frac{\left(I_{green} - I_{blue}\right)_t - \left(I_{green} - I_{blue}\right)_{PBS}}{\left(I_{green} - I_{blue}\right)_{t\,=\,0,\,crySI} - \left(I_{green} - I_{blue}\right)_{PBS}} \quad (3)$$

where I_{green} and I_{blue} represents the integrated intensity of the green and blue channel, respectively.

2.8. Intra-vitreal pharmacokinetics

To evaluate the pharmacokinetics of crySI relative to that of mini cry and SI, mice were administered 100pmol (1 μE, 100 μM) fluorescein-labeled peptide through intra-vitreal injection. The mice were euthanized at selected time points (0.25, 1, 2.7, 8h, 1, 3, 6, 9 and 13 days). Eyes were enucleated and immediately frozen at – 80 °C with 100 μE RIPA buffer containing protease/phosphatase inhibitor. On the last day of experiment, all samples collected previously were thawed, homogenized using a PRO200 homogenizer (PRO Scientific Inc., Oxford, CT), and centrifuged. Fluorescence concentration in the supernatant was determined using a calibrated fluorescence microplate assay run on a Synergy H1 Hybrid Multi Mode Microplate Reader (BioTek, Winooski, VT). The average background fluorescence of eyeballs injected with only PBS was measured and subtracted from the sample data.

2.9. Pharmacokinetic analysis

Since both crySI and SI followed a bi-exponential elimination from the eye, the total amount [pmoles], X_t, of recovered fluorescence for mini cry, crySI, and SI as a function of time [days], t, was fit to the following decay curve:

$$X_t = X_0 f_{fast} e^{-k_{fast}t} + X_0\left(1 - f_{fast}\right)e^{-k_{slow}t} \quad (4)$$

where f_{fast} is the fraction of the dose that cleared rapidly, X_0 is the initial amount of dose detected in the eye at time based on the fit, k_{fast} is a first order rate constant fitting rapid

elimination, and k_{slow} is a first order rate constant fitting slower elimination. Only one rate of decay was observed for mini cry; therefore, f_{fast} was fixed at 1. As a measure of relative ocular exposure, the AUC (area under the curve) and AUMC (area under the moment curve) were estimated using the trapezoidal rule, which was used to determine the mean residence time (MRT).

2.10. Retinal histology

Cryostat sections (8 μm) of snap-frozen posterior eye-cups were obtained from groups injected with crySI, SI, mini cry, or PBS 7 days and 30 days after $NaIO_3$ challenge. After fixation with 4% paraformaldehyde for 30 min, standard equatorial sections of posterior eye cup through the optic nerve were prepared for hematoxylin and eosin (H&E) staining and imaged with Aperio digital pathology slide scanner (Leica Biosystems, Buffalo Grove, IL).

2.11. TUNEL staining

In Situ Cell Death Detection Kit for the terminal deoxynucleotide transferase dUTP nick end labeling (TUNEL) assay was performed on retinal sections according to the manufacturer's instructions. Retinal sections (8 μm) were fixed in 4% paraformaldehyde (PFA) and permeabilized with 0.1% Triton X-100. The sections were incubated with the TUNEL reaction mixture that contains TdT and TMR-dUTP for 1 h at 37 °C in a humidified chamber in the dark. After washing, the label incorporated at sites of DNA damage was visualized by fluorescence microscopy. TUNEL-positive cells were counted and data were expressed as percent of total cells undergoing cell death [39].

2.12. Immunofluorescence staining

Sections were fixed in 4% PFA and permeabilized with 0.1% Triton X-100. Samples were blocked with 5% normal goat serum for 30 min. Sections were incubated with either rabbit antibody against cleaved caspase-3 (1:100 dilution) or rabbit antibody against αB crystallin (1:100 dilution) overnight. Sections were then incubated with goat fluorescein-conjugated anti-rabbit secondary antibody for 30 min. Images were obtained using a Keyence fluorescence digital microscope. (Keyence, Itasca, IL). For quantification of immunofluorescence, digital images were analyzed (n = 5–7), and the average total corrected fluorescence (background subtracted) was calculated using ImageJ (US NIH, Bethesda, MD) [40].

2.13. Data analysis

Data presented are representative curves or mean ± SD. All experiments were repeated at least three times. Statistical analyses were performed by a Student *t*-test and a one-way ANOVA followed by Tukey's post-hoc test using Prism (GraphPad Software, La Jolla, CA). A p value of < 0.05 was considered statistically significant.

3. Results

3.1. crySI, which carries an αB crystallin peptide (mini cry), protects mouse RPE from $NaIO_3$-induced degeneration

To evaluate the relative protection of crySI or mini cry against RPE loss and degeneration, eyes were pre-treated by intra-vitreal injection of crySI, SI, or mini cry (Table 1) prior to $NaIO_3$ challenge as described in Fig. 1. Fundus photographs were taken prior to enucleation and the percent retinal degeneration was compared. Fig. 2A shows that eyes challenged with $NaIO_3$ and treated with PBS had large areas of retinal degeneration (> 50%) compared to unchallenged controls. In contrast, mice given a single intra-vitreal injection of crySI between two to fourteen days before challenge had significantly lower retinal degeneration (< 25%) compared to mice treated with mini cry (Fig. 2B, C). Intra-vitreal administration of SI alone had no effect on the area of $NaIO_3$ induced degeneration. When retinal sections from these groups were imaged by H&E staining, there appears significant tissue disruption in all $NaIO_3$ challenged mice; furthermore, only crySI consistently protected against this disruption (Fig. 2D). In the $NaIO_3$ model, the RPE/Bruch's membrane was discontinuous with patchy RPE loss and irregular degenerated cell aggregates (see arrows). The outer nuclear layer (ONL) was clearly distorted and its thickness was substantially reduced compared to the control animals (see arrows). There was marked loss of photoreceptor inner and outer segments. The thickness of the RPE layer, ONL, and inner nuclear layer (INL) were also distorted in mini cry treated retinas when compared to crySI treated retinas. Further there was significant thinning of ONL in mini cry injected groups, which appeared almost normal in crySI treated retinas. Similar protection of the retina was observed only for eyes pre-treated with crySI by 1 and 2 weeks prior to $NaIO_3$ challenge (Figs. S1, S2).

3.2. crySI has extended ocular retention following intra-vitreal administration

Unlike free mini cry, crySI assembles coacervates above ~30 °C, which raised the possibility that it has a different disposition in the eye [35]. Having determined that crySI is neuroprotective for at least two weeks prior to $NaIO_3$ challenge (Fig. 2C), we hypothesized that ELP- mediated assembly of crySI may extend retention near the retina. To test this hypothesis, the pharmacokinetics of crySI relative to mini cry and SI was evaluated by injecting fluorescently-labeled samples (Fig. 3A) into the mouse vitreous and monitoring the total fluorescence in whole, enucleated eyeballs for up to 2 weeks. Consistent with peptides of low molecular weight (2.8 kD), labeled mini cry was undetectable in the ocular compartment within 3 days (Fig. 3B); furthermore, quantification of its removal suggests that it cleared from the eye by a mono-exponential decay and has a mean residence time of 0.4 days (Table 2). In contrast, both crySI and SI were cleared from the eye by biexponential decay, with a much slower mean residence times of 3.0 and 3.4 days, respectively. Ocular exposure to crySI as measured by the area under curve (AUC) of the fluorescein amount was increased by 4 times from 14.5 pmol*days for mini cry to 56.2 pmol*days for crySI. To confirm differences in ocular pharmacokinetics using a non-invasive approach, color fundus imaging was used to excite the fluorescent dye and photograph each mouse retina over time (Figs. 3C, S3). Most of the mini cry signal was cleared from the vitreous within one week after injection, while crySI and SI remained easily visible in the fundus after 2 weeks (Fig. 3D). Furthermore, the crySI microparticles were observed in the vitreous above the retina

using confocal imaging (Fig. S4). Taken together, these studies indicate that ELP-mediated peptide assembly significantly increases the duration of crySI exposure to the retina after intra-vitreal administration.

3.3. crySI suppresses $NaIO_3$ induced cell death

In our previous report, crySI was strongly protective against oxidation-induced cell death in cultured human RPE cells [35]. Based on the significant protection observed *in vivo* for $NaIO_3$ challenged mice (Fig. 2), the TUNEL assay was used to characterize cell death in retinas with both short (2-day pre-treatment and one week $NaIO_3$ challenge) and long (2-week pre-treatment and one month $NaIO_3$ challenge) term treatment (Fig. 4). $NaIO_3$ challenge induced a high degree of TUNEL positive cells (~20–25%) for groups pre-treated with PBS or SI controls. The mini cry treated samples did not significantly decrease apoptotic cell death when compared to the PBS in two days or two weeks pretreated groups. (Fig. 4A, B). In contrast, crySI treated eyes had significantly lower (< 5%, $p < 0.001$) percentages of TUNEL positive cells in both groups. TUNEL-positive cells (red) were mostly seen in the ONL, RPE and choroid region; furthermore, these regions showed less disruption *via* a nuclear stain (DAPI). This observation suggests that the extended ocular retention in the retina compared to free mini cry may play a factor in its level of protection (Fig. 3).

3.4. crySI treatment reduces activation of caspase-3

Having demonstrated that crySI suppresses retinal cell death upon $NaIO_3$ challenge, retina sections were next assessed for the key executioner caspase of conventional cell death, cleaved caspase-3, using immunofluorescence. Consistent with protection against TUNEL staining (Fig. 4), the fluorescence intensity for cleaved caspase-3 was greatly reduced in crySI treated eyes as compared to all other groups with both short- and long-term treatments (Fig. 5). The quantification of relative fluorescence intensities against PBS treated group revealed a significantly ($p < 0.0001$) lower level of activated caspase-3 in the RPE layer for eyes treated with crySI *vs.* mini cry and SI. Collectively, these results confirm that crySI, and not free mini cry, induces strong protection of RPE through the canonical caspase-3 pathway.

3.5. Prior to its clearance, crySI treatment increases staining for total αB crystallin

Overexpression of αB crystallin is known to protect cells from ROS induced oxidative stress and inflammation, while knocking out αB crystallin make cells more susceptible [41,42]. To determine whether retinal degeneration induced by $NaIO_3$ was associated with changes in αB crystallin, challenged retinas were probed with an antibody to detect endogenous and exogenous crystallin (Fig. S5). For eyes treated two days prior $NaIO_3$ challenge, crySI significantly ($p < 0.0001$) enhanced the detection of total αB crystallin compared to other groups by increasing the staining in RPE, photoreceptors and inner nuclear layer (Fig. 6A), which is consistent with the distribution of fluorescently-labeled crySI observed in the retina (Fig. S4). In contrast, no significant differences were observed in retinas after long-term treatment, which were collected 6 weeks (2-week pretreatment followed by one-month challenge) post administration (Fig. 6A). This is consistent with the collected

pharmacokinetic data (Fig. 3, Table 2), which suggests that by 6 weeks (~14 terminal half-lives) the majority of exogenous crySI was cleared from the retina.

4. Discussion

This study demonstrates the ability of an ELP to deliver through intra-vitreal administration a cytoprotective 20-mer αB crystallin peptide *in vivo* and significantly rescue a murine model of retinal degeneration (Figs. 2, S1, S2) by inhibiting caspase-3 mediated cell death (Figs. 5, 6). Protection was also associated with extended retention of crySI for at least two weeks (Fig. 3) while the free mini cry peptide was removed in < 2 days (Figs. 3B, S3). To the best of our knowledge, this is the first study to demonstrate the protective actions of ELP-fused αB crystallin peptide in any retinal neurodegeneration mouse models. These findings demonstrate potent protective potential for ELP-crystallin fusions in the outer retina caused by oxidative stress, a salient feature of GA that primarily involves RPE atrophy followed by photoreceptor degeneration.

Thought to be a primary cause of AMD, oxidative stress is associated with RPE dysfunction, photoreceptor death, and retinal degeneration [43,44]. For eyes with dry AMD, increased αB crystallin expression is more frequent in RPE cells and usually occurs in the early stages of AMD [45]. Proteomic analysis showed αB crystallin to be a major protein constituent of AMD-associated drusen, which are subretinal protein and lipid-rich extracellular deposits [46], pointing to the significance of this protein in AMD etiology. Given the above observations, and because of its known multiple functions in the eye, this manuscript explores the protective potential of intra-vitreal αB crystallin in a murine model of GA. Intra-venous administration of $NaIO_3$ induces patchy loss of RPE, which leads to degeneration of the photoreceptor layer and thinning/distortion of the outer nuclear layer (Fig. 2D). Since systemic $NaIO_3$ challenge recapitulates many key features of dry AMD, such as oxidative stress, inflammation, and RPE dysfunction, this model is now widely used to study GA [4,6]. In the present study, 33 mg/kg BW $NaIO_3$ induced significant degeneration (over 50%) of the RPE layer and neural retinal distortion within a week. Previous studies showed that even lower doses of $NaIO_3$ cause αB crystallin deficiency and retinal damage [6], suggesting the importance of this small heat shock protein in RPE survival. To date, studies in multiple disease models reveal that administration of recombinant αB crystallin protects from encephalomyelitis, ischemic optic neuropathy, stroke, and myocardial infarction [17,18,20,47]. More recently, our team showed that a 20-mer, corresponding to residues 73–92 of human αB crystallin, is sufficient to protect RPE cells from oxidative stress-induced cell death [27,35]. This 20-mer was also effective in protecting against experimental encephalomyelitis [28].

Recent therapeutic strategies for the treatment of dry AMD target inflammation and complement activation, suppress oxidative stress, or provide neuroprotection. Since αB crystallin elicits all these functions under multiple in *vitro* and *in vivo* patho-physiological conditions, it may be an ideal candidate for therapy. Unfortunately, frequent dosing was required for previous *in vivo* pre-clinical studies owing to the low retention time and relative bioavailability of recombinant αB crystallin [28], which is not clinically applicable for intra-vitreal administration and may cause poor patient compliance. To overcome this critical

limitation, we previously used a synthetic polymer polycaprolactone (PCL) to encapsulate mini cry and deliver it to cultured RPE cells, where low doses efficiently resulted in cellular protection [27]. PCL has been widely used as a biomaterial due to its low immunogenicity and high biocompatibility. However, drawbacks related to polydispersity, encapsulation stability, burst release, and limited degradation limit the application of this platform [48]. To overcome these limitations, our team developed a self-assembling mini cry-ELP fusion containing the hydrophobic ELP $(Val\text{-}Pro\text{-}Gly\text{-}Ile\text{-}Gly)_{48}$, which modulates its nanoassembly, cellular uptake, and bioactivity [35]. Compared to PCL, ELPs are derived from human tropoelastin and can be generated *via* genetic engineering and recombinant biosynthesis, which offers an exquisite level of precision and tunability with regards to the length, molecular weight, sequence and monodispersity of the resulting material. Most importantly, ELPs have the advantage of being thermo-responsive and can be tailored to assemble coacervates at body temperature while maintaining the activity of fusion proteins [37,49–51]. At physiological temperatures, the hydrophobic ELP phase separates and forms a depot in the vitreous capsule (Fig. S4), which correlates with an increased exposure (Area Under the Curve, AUC) for the fused αB crystallin peptide compared to that of 20-mer αB crystallin (Table 2) that reduces the retinal response to $NaIO_3$ challenge (Fig. 2). While the 20-mer αB crystallin alone was undetectable after 2 days, (Fig. S3), crySI was easily detectable even after 2 weeks (Fig. 3B, C). It has been reported that the serological blood half-life for intact αB crystallin is on the order of 6 h; however, the systemic half-life for free mini cry peptide would be much shorter and would not guarantee access to the retina [28]. Concurrent with the assembly of a nanostructure, crySI remains bioactive and retains both chaperone and anti-apoptotic functions [35], which suggests its potential for treatment of retinal degeneration and other inflammatory disorders. These findings corroborate other reports such as for SynB1-ELP1-Dox, which has a longer systemic circulation than free drug [52]. In short, the cumulative effect of improved intraocular pharmacokinetics, and long-term retention of crySI compared to mini cry may explain the significant efficacy of crySI to protect the retina from oxidative stress.

The observation that crySI is more effective than soluble mini cry peptide is of additional significance in the light of potential clinical application in humans. Preclinical explorations of ELPs support their use as macromolecules to enhance half-life of peptides or small proteins. Our previous study showed that cellular uptake of the thermally sensitive crySI was enhanced in stressed RPE cells compared with the uptake of the same polypeptide in control cells [35]. Further, in this report we demonstrate that ELPs are retained in one target tissue for durations as long as two weeks. In addition, by leveraging intra-vitreal administration the likelihood of off-target drug effects will be minimized as recently reported for intranasal delivery [53]. Previous studies have demonstrated that apoptosis plays an important role in RPE degeneration in $NaIO_3$ challenged mice, and that αB crystallin has anti-apoptotic effects [4,6,27,35,39]. In human RPE cells treated with low doses of $NaIO_3$, RPE apoptosis was induced *via* upregulating mitochondrial ROS and subsequent activation of downstream caspase activity [6]. We have demonstrated in the present study that in mice with retinal degeneration, the number of TUNEL-positive cells and the activation of caspase-3 were significantly reduced in crySI-treated eyes compared to PBS/SI/mini cry, consistent with its

protective role. The less significant protection offered by mini cry may be attributed to the bioavailability and fast clearance from the eye.

While ELPs have demonstrated high biocompatibility and low immunogenicity in animal models [54–56] and human clinical trials (PhaseBio Inc.), additional evidence for their immunological effect in the eye was obtained by staining for infiltration of CD3+ T cells in the retina for mice exposed to either short- or long-term treatment of ELPs (Fig. S6). No positive staining was observed in either SI or crySI treated eyes. Given the bioactivity of crySI in a murine model, we further assessed its clinical potential in an in *vitro* culture model relevant to the human retina. Our team developed an excellent working model where human fetal RPE cells form polarized monolayers that have features of their *in vivo* counterparts [57–59]. Polarization is one of the salient features of the differentiated phenotype of the RPE monolayer permitting attachment to Bruch's membrane, formation of the outer-retina-barrier, and specialization of the RPE cells' apical surface for phagocytosis of shed rod outer segments. Furthermore, RPE cells are essential transporters of water, electrolytes, and nutrients between the choroid and the neural retina. RPE monolayers also provide trophic guidance to both photoreceptors and choroid through the polarized secretion of trophic growth factors. To corroborate the observation that crySI protects RPE in a mouse model of oxidative challenge (Fig. 2), studies with polarized RPE monolayers reveal that 2.5 mM $NaIO_3$ challenge results in a significant loss of transepithelial resistance (TER), which was associated with a disruption in tight junctions as indicated by ZO-1 (Fig. S7). Only treatment with crySI maintained TER and restored tight junction morphology, suggesting that part of the protection observed in the mouse model of GA may be due to direct protection of the RPE integrity. We also compared different doses of mini cry in the same primary culture model; furthermore, an ~6 fold higher concentration of mini cry was required to reach the same protection offered by crySI. This observation is consistent with our previous report that crySI is more efficient in arresting oxidant-induced apoptosis than the free mini cry peptide (Fig. S7C). Thus, both human and mouse models of oxidative stress in the RPE support the protective potential of αB crystallin ELP fusions in dry AMD. However, the exact mechanisms underlying how crySI distributes, permeates retina, exerts cytoprotective function and degrades in the vitreous remain to be investigated.

5. Conclusion

In summary, this *in vivo* study shows that intra-vitreal injection of crySI attenuates $NaIO_3$ induced retinal degeneration in mice by rescuing RPE and preventing disruption of other retinal layers, specifically the ONL *via* suppression of the effects of oxidative stress. Unlike the free mini cry peptide, crySI has potential to protect against the progression of AMD because the ELP causes it to be retained in the vitreous capsule where it can protect for at least 2 weeks. CrySI blocks oxidative stress induced cell death, which protects the RPE monolayer integrity. Taken together, these data provide the first *in vivo* proof-of-concept for the use of ELPs to modulate cytoprotective peptides for treating the eye *via* intra-vitreous administration, however, a more thorough understanding of the mechanisms of ELP fusions in the vitreous is necessary for their further development as possible treatments for AMD or other diseases of the retina.

Supplementary Material

Refer to Web version on PubMed Central for supplementary material.

Acknowledgement

This work was supported by RO1EY01545, the L.K. Whittier foundation, the Gavin S. Herbert Endowed Chair of Pharmaceutical Sciences, the Arnold and Mabel Beckman Foundation, and USC Clinical and Translational Science Institute SC CTSI (NIH/NCRR/NCATS) Grant # UL1TR000130.

Abbreviations:

AMD	Age-related macular degeneration
RPE	Retinal pigment epithelium
ELP	Elastin-like polypeptide
GA	Geographic atrophy
$NaIO_3$	Sodium iodate
mini cry	20- mer αB crystallin
crySI	20-mer αB crystallin fused with ELP
ROI	Region of interest
PFA	Paraformaldehyde
sHSPs	small heat shock proteins
TER	Transepithelial electrical resistance
AUC	Area under the curve
AUMC	Area under the moment curve
MRT	Mean residence time

References

[1]. Bird AC, Therapeutic targets in age-related macular disease, J. Clin. Invest 120 (2010) 3033–3041. [PubMed: 20811159]

[2]. Klein ML, Ferris FL, Armstrong J, Hwang TS, Chew EY, Bressler SB, Chandra SR, Retinal precursors and the development of geographic atrophy in age- related macular degeneration, Ophthalmology 115 (2008) 1026–1031. [PubMed: 17981333]

[3]. Wright CB, Ambati J, Dry Age-Related Macular Degeneration Pharmacology, Pharmacologic Therapy of Ocular Disease, Springer, 2016, pp. 321–336.

[4]. Franco LM, Zulliger R, Wolf-Schnurrbusch UE, Katagiri Y, Kaplan HJ, Wolf S, Enzmann V, Decreased visual function after patchy loss of retinal pigment epithelium induced by low-dose sodium iodate, Invest. Ophthalmol. Vis. Sci 50 (2009) 4004–4010. [PubMed: 19339739]

[5]. Enzmann V, Row BW, Yamauchi Y, Kheirandish L, Gozal D, Kaplan HJ, McCall MA, Behavioral and anatomical abnormalities in a sodium iodate-induced model of retinal pigment epithelium degeneration, Exp. Eye Res 82 (2006) 441–448. [PubMed: 16171805]

[6]. Zhou P, Kannan R, Spee C, Sreekumar PG, Dou G, Hinton DR, Protection of retina by Ab Crystallin in sodium iodate induced retinal degeneration, PLoS One 9 (2014) e98275. [PubMed: 24874187]

[7]. Kannan R, Hinton DR, Sodium iodate induced retinal degeneration: new insights from an old model, Neural Regen. Res 9 (2014) 2044. [PubMed: 25657718]

[8]. Nilsson SEG, Knave B, Persson HE, Changes in ultrastructure and function of the sheep pigment epithelium and retina induced by sodium iodate, Acta Ophthalmol 55 (1977) 1007–1026. [PubMed: 579541]

[9]. Obata R, Yanagi Y, Tamaki Y, Hozumi K, Mutoh M, Tanaka Y, Retinal degeneration is delayed by tissue factor pathway Inhibitor-2 in Rcs rats and a sodium-iodate-induced model in rabbits, Eye 19 (2005) 464. [PubMed: 15184935]

[10]. Yang Y, Qin YJ, Yip YW, Chan KP, Chu KO, Chu WK, Ng TK, Pang CP, Chan SO, Green tea catechins are potent anti-oxidants that ameliorate sodium iodate-induced retinal degeneration in rats, Sci. Rep 6 (2016) 29546. [PubMed: 27383468]

[11]. Wang J, Iacovelli J, Spencer C, Saint-Geniez M, Direct effect of sodium iodate on neurosensory retina, Invest. Ophthalmol. Vis. Sci 55 (2014) 1941–1953. [PubMed: 24481259]

[12]. Zhang X-Y, Ng TK, Brelén ME, Wu D, Wang JX, Chan KP, Yung JSY, Cao D, Wang Y, Zhang S, Continuous exposure to non-lethal doses of sodium iodate induces retinal pigment epithelial cell dysfunction, Sci. Rep 6 (2016) 37279. [PubMed: 27849035]

[13]. Kannan R, Sreekumar PG, Hinton DR, Novel roles for A-Crystallins in retinal function and disease, Prog. Retin. Eye Res 31 (2012) 576–604. [PubMed: 22721717]

[14]. Yaung J, Jin M, Barron E, Spee C, Wawrousek EF, Kannan R, Hinton DR, A-Crystallin distribution in retinal pigment epithelium and effect of gene knockouts on sensitivity to oxidative stress, Mol. Vis 13 (2007) 566. [PubMed: 17438522]

[15]. Masilamoni J, Jesudason E, Baben BJ, Jebaraj CE, Dhandayuthapani S, Jayakumar R, Molecular chaperone A-Crystallin prevents detrimental effects of Neuroinflammation, Biochimica et Biophysica Acta (BBA)-Molecular Basis of Disease 1762 (2006) 284–293. [PubMed: 16443350]

[16]. van Noort JM, Bsibsi M, Nacken PJ, Gerritsen WH, Amor S, Holtman IR, Boddeke E, van Ark I, Leusink-Muis T, Folkerts G, Activation of an immune-regulatory macrophage response and inhibition of lung inflammation in a mouse model of Copd using heat-shock protein alpha B-Crystallin-loaded Plga microparticles, Biomaterials 34 (2013) 831–840. [PubMed: 23117214]

[17]. Ousman SS, Tomooka BH, Van Noort JM, Wawrousek EF, O'Conner K, Hafler DA, Sobel RA, Robinson WH, Steinman L, Protective and therapeutic role for Ab-Crystallin in autoimmune demyelination, Nature 448 (2007) 474. [PubMed: 17568699]

[18]. Pangratz-Fuehrer S, Kaur K, Ousman S, Steinman L, Liao Y, Functional Rescue of Experimental Ischemic Optic Neuropathy with Ab-Crystallin, Eye 25 (2011) 809. [PubMed: 21475310]

[19]. Velotta JB, Kimura N, Chang SH, Chung J, Itoh S, Rothbard J, Yang PC, Steinman L, Robbins RC, Fischbein MP, Ab-Crystallin improves murine cardiac function and attenuates apoptosis in human endothelial cells exposed to ischemia-reperfusion, Ann. Thorac. Surg 91 (2011) 1907–1913. [PubMed: 21619989]

[20]. Arac A, Brownell SE, Rothbard JB, Chen C, Ko RM, Pereira MP, Albers GW, Steinman L, Steinberg GK, Systemic augmentation of Ab-Crystallin provides therapeutic benefit twelve hours post-stroke onset via immune modulation, Proc. Natl. Acad. Sci 108 (2011) 13287–13292. [PubMed: 21828004]

[21]. Klopstein A, Santos-Nogueira E, Francos-Quijorna I, Redensek A, David S, Navarro X, López-Vales R, Beneficial effects of Ab-Crystallin in spinal cord contusion injury, J. Neurosci 32 (2012) 14478–14488. [PubMed: 23077034]

[22]. Bhattacharyya J, Udupa E. Padmanabha, Wang J, Sharma KK, Mini-Ab-Crystallin: a functional element of Ab-Crystallin with chaperone-like activity, Biochemistry 45 (2006) 3069–3076. [PubMed: 16503662]

[23]. Raju M, Santhoshkumar P, Sharma KK, Alpha-Crystallin-derived peptides as therapeutic chaperones, Biochimica et Biophysica Acta (BBA)-General Subjects 1860 ((2016) 246–251. [PubMed: 26141743]

[24]. Ghosh JG, Estrada MR, Clark JI, Interactive domains for chaperone activity in the small heat shock protein, human Ab Crystallin, Biochemistry 44 (2005) 14854–14869. [PubMed: 16274233]

[25]. Ghosh JG, Houck SA, Clark JI, Interactive sequences in the stress protein and molecular chaperone human Ab Crystallin recognize and modulate the assembly of filaments, Int. J. Biochem. Cell Biol 39 (2007) 1804–1815. [PubMed: 17590381]

[26]. Clark JI, Functional sequences in human Alphab Crystallin, Biochimica et Biophysica Acta (BBA)-General Subjects 1860 (2016) 240–245. [PubMed: 26341790]

[27]. Sreekumar PG, Chothe P, Sharma KK, Baid R, Kompella U, Spee C, Kannan N, Manh C, Ryan SJ, Ganapathy V, Antiapoptotic properties of A-Crystallin-derived peptide chaperones and characterization of their uptake transporters in human Rpe cells, Invest. Ophthalmol. Vis. Sci 54 (2013) 2787–2798. [PubMed: 23532520]

[28]. Kurnellas MP, Brownell SE, Su L, Malkovskiy AV, Rajadas J, Dolganov G, Chopra S, Schoolnik GK, Sobel RA, Webster J, Chaperone activity of small heat shock proteins underlies therapeutic efficacy in experimental autoimmune encephalomyelitis, J. Biol. Chem 287 (2012) 36423–36434. [PubMed: 22955287]

[29]. Fosgerau K, Hoffmann T, Peptide therapeutics: current status and future directions, Drug Discov. Today 20 (2015) 122–128. [PubMed: 25450771]

[30]. Kim H, Csaky KG, Nanoparticle-integrin antagonist C16y peptide treatment of Choroidal neovascularization in rats, J. Control. Release 142 (2010) 286–293. [PubMed: 19895863]

[31]. Ghosh JG, Nguyen AA, Bigelow CE, Poor S, Qiu Y, Rangaswamy N, Ornberg R, Jackson B, Mak H, Ezell T, Long-acting protein drugs for the treatment of ocular diseases, Nat. Commun 8 (2017) 14837. [PubMed: 28332616]

[32]. Li H, Tran VV, Hu Y, Saltzman WM, Barnstable CJ, Tombran-Tink J, A Pedf N-terminal peptide protects the retina from ischemic injury when delivered in Plga nanospheres, Exp. Eye Res 83 (2006) 824–833. [PubMed: 16822505]

[33]. Borhani H, Peyman GA, Rahimy MH, Thompson H, Suppression of experimental proliferative vitreoretinopathy by sustained intraocular delivery of 5-Fu, Int. Ophthalmol 19 (1995) 43–49. [PubMed: 8537196]

[34]. Bisht R, Rupenthal ID, Plga nanoparticles for Intravitreal peptide delivery: statistical optimization, Characterization and Toxicity Evaluation, Pharmaceutical Development Technology (2016) 1–10.

[35]. Wang W, Sreekumar PG, Valluripalli V, Shi P, Wang J, Lin Y-A, Cui H, Kannan R, Hinton DR, MacKay JA, Protein polymer nanoparticles engineered as chaperones protect against apoptosis in human retinal pigment epithelial cells, J. Control. Release 191 (2014) 4–14. [PubMed: 24780268]

[36]. Roberts S, Dzuricky M, Chilkoti A, Elastin-like polypeptides as models of intrinsically disordered proteins, FEBS Lett. 589 (2015) 2477–2486. [PubMed: 26325592]

[37]. Gilroy CA, Luginbuhl KM, Chilkoti A, Controlled release of biologics for the treatment of type 2 diabetes, J. Control. Release 240 (2016) 151–164. [PubMed: 26655062]

[38]. Tang XN, Berman AE, Swanson RA, Yenari MA, Digitally quantifying cerebral hemorrhage using Photoshop® and Image J, J. Neurosci. Methods 190 (2010) 240–243. [PubMed: 20452374]

[39]. Sreekumar PG, Kannan R, Kitamura M, Spee C, Barron E, Ryan SJ, Hinton DR, Ab crystallin is apically secreted within exosomes by polarized human retinal pigment epithelium and provides neuroprotection to adjacent cells, PLoS One 5 (2010) e12578. [PubMed: 20949024]

[40]. Burgess A, Vigneron S, Brioudes E, Labbé J-C, Lorca T, Castro A, Loss of human Greatwall results in G2 arrest and multiple mitotic defects due to deregulation of the cyclin B-Cdc2/Pp2a balance, Proc. Natl. Acad. Sci 107 (2010) 12564–12569. [PubMed: 20538976]

[41]. Yaung J, Kannan R, Wawrousek EF, Spee C, Sreekumar PG, Hinton DR, Exacerbation of retinal degeneration in the absence of alpha crystallins in an in vivo model of chemically induced hypoxia, Exp. Eye Res 86 (2008) 355–365. [PubMed: 18191123]

[42]. Sreekumar PG, Spee C, Ryan SJ, Cole SP, Kannan R, Hinton DR, Mechanism of Rpe cell death in A-Crystallin deficient mice: a novel and critical role for Mrp1-mediated Gsh efflux, PLoS One 7 (2012) e33420. [PubMed: 22442691]

[43]. Ambati J, Fowler BJ, Mechanisms of age-related macular degeneration, Neuron 75 (2012) 26–39. [PubMed: 22794258]

[44]. Rickman CB, Farsiu S, Toth CA, Klingeborn M, Dry age-related macular degeneration: mechanisms, therapeutic targets, and imaging, Invest. Ophthalmol. Vis. Sci 54 (2013) ORSF68–ORSF80. [PubMed: 24335072]

[45]. De S, Rabin DM, Salero E, Lederman PL, Temple S, Stern JH, Human retinal pigment epithelium cell changes and expression of Ab-Crystallin: a biomarker for retinal pigment epithelium cell change in age-related macular degeneration, Arch. Ophthalmol 125 (2007) 641–645. [PubMed: 17502503]

[46]. Crabb JW, Miyagi M, Gu X, Shadrach K, West KA, Sakaguchi H, Kamei M, Hasan A, Yan L, Rayborn ME, Drusen proteome analysis: an approach to the etiology of age-related macular degeneration, Proc. Natl. Acad. Sci 99 (2002) 14682–14687. [PubMed: 12391305]

[47]. Rothbard JB, Kurnellas MP, Brownell S, Adams CM, Su L, Axtell RC, Chen R, Fathman CG, Robinson WH, Steinman L, Therapeutic effects of systemic Administration of Chaperone Ab-Crystallin Associated with binding Proinflammatory plasma proteins, J. Biol. Chem 287 (2012) 9708–9721. [PubMed: 22308023]

[48]. Ulery BD, Nair LS, Laurencin CT, Biomedical applications of biodegradable polymers, J. Polym. Sci. B Polym. Phys 49 (2011) 832–864. [PubMed: 21769165]

[49]. Gilroy CA, Roberts S, Chilkoti A, Fusion of fibroblast growth factor 21 to a thermally responsive biopolymer forms an injectable depot with sustained antidiabetic action, J. Control. Release 277 (2018) 154–164. [PubMed: 29551712]

[50]. Janib SM, Pastuszka M, Aluri S, Folchman-Wagner Z, Hsueh P, Shi P, Lin Y, Cui H, Mackay J, A quantitative recipe for engineering protein polymer nanoparticles, Polym. Chem 5 (2014) 1614–1625. [PubMed: 24511327]

[51]. Despanie J, Dhandhukia JP, Hamm-Alvarez SF, MacKay JA, Elastin-like polypeptides: therapeutic applications for an emerging class of nanomedicines, J. Control. Release 240 (2016) 93–108. [PubMed: 26578439]

[52]. Moktan S, Perkins E, Kratz F, Raucher D, Thermal targeting of an acid-sensitive doxorubicin conjugate of elastin-like polypeptide enhances the therapeutic efficacy compared with the parent compound in vivo, Mol. Cancer Ther. 11 (2012) 1547–1556. [PubMed: 22532601]

[53]. Mcgowan JW, Shao Q, Vig PJ, Bidwell GL, III, Intranasal administration of Elastin-like polypeptide for therapeutic delivery to the central nervous system, Drug Design, Development and Therapy 10 (2016) 2803.

[54]. Megeed Z, Cappello J, Ghandehari H, Genetically engineered silk-elastinlike protein polymers for controlled drug delivery, Adv. Drug Deliv. Rev 54 (2002) 1075–1091. [PubMed: 12384308]

[55]. Cho S, Dong S, Parent K, Chen M, Immune-tolerant elastin-like polypeptides (Iteps) and their application as Ctl vaccine carriers, J. Drug Target 24 (2016) 328–339. [PubMed: 26307138]

[56]. Cappello J, Crissman J, Crissman M, Ferrari F, Textor G, Wallis O, Whitledge J, Zhou X, Burman D, Aukerman L, In-situ self-assembling protein polymer gel systems for administration, delivery, and release of drugs, J. Control. Release 53 (1998) 105–117. [PubMed: 9741918]

[57]. Sonoda S, Spee C, Barron E, Ryan SJ, Kannan R, Hinton DR, A protocol for the culture and differentiation of highly polarized human retinal pigment epithelial cells, Nat. Protoc 4 (2009) 662. [PubMed: 19373231]

[58]. Sreekumar PG, Zhou J, Sohn J, Spee C, Ryan SJ, Maurer BJ, Kannan R, Hinton DR, N-(4-Hydroxyphenyl) retinamide augments laser-induced choroidal neovascularization in mice, Invest. Ophthalmol. Vis. Sci 49 (2008) 1210–1220. [PubMed: 18326751]

[59]. Sreekumar PG, Ishikawa K, Spee C, Mehta HH, Wan J, Yen K, Cohen P, Kannan R, Hinton DR, The mitochondrial-derived peptide humanin protects Rpe cells from oxidative stress, senescence, and mitochondrial dysfunction, Invest. Ophthalmol. Vis. Sci 57 (2016) 1238–1253. [PubMed: 26990160]

[60]. Zhu D, Sreekumar PG, Hinton DR, Kannan R, Expression and regulation of enzymes in the ceramide metabolic pathway in human retinal pigment epithelial cells and their relevance to retinal degeneration, Vis. Res 50 (2010) 643–651. [PubMed: 19765607]

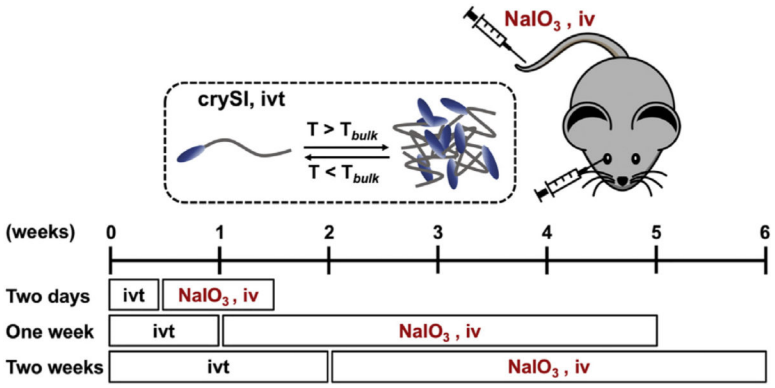

Fig. 1.

Schematic demonstrating the iodate challenge study design. A thermos-responsive fusion protein (crySI) containing a 20-mer αB crystallin peptide was evaluated for its protective potential in a mouse model of AMD. Three independent studies were performed to assess the short- and long-term protection of crySI. Two days: 2-day pretreatment followed by one week $NaIO_3$ challenge; One week: 1-week pretreatment followed by one-month $NaIO_3$ challenge; Two weeks: 2-week pretreatment followed by one-month $NaIO_3$ challenge, iv: intravenous, ivt: intra-vitreal

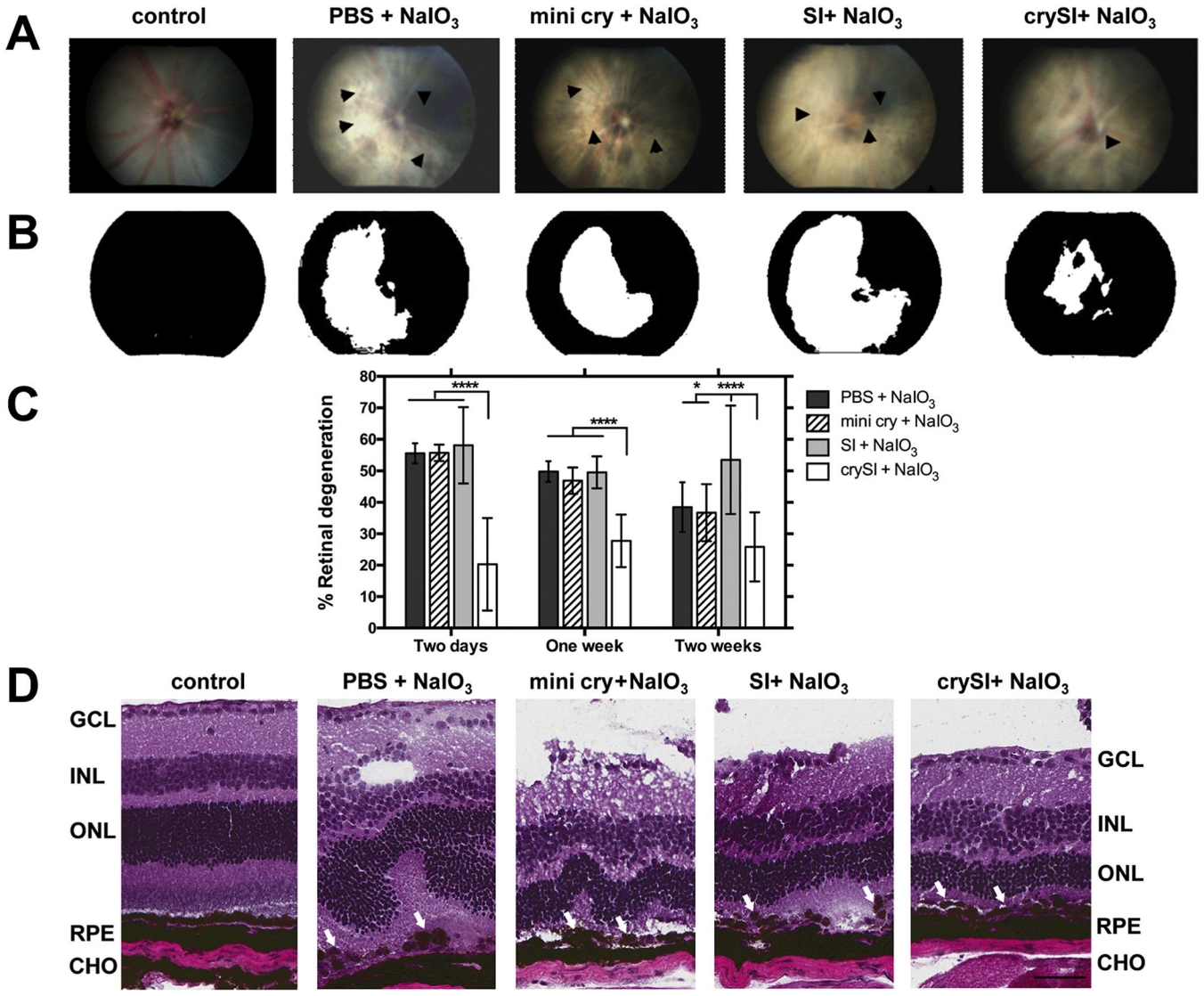

Fig. 2.

Intra-vitreal crySI protects against retinal degeneration caused by $NaIO_3$ challenge in *129S6/SvEvTac* mice. (A) Color fundus photography was used to compare therapeutic efficacy of crySI with controls in the mouse retina. Mice were pre-treated with 2 μL into the vitreous chamber with PBS, SI, crySI, or mini cry (250 μM) two days prior to intra-venous challenge with $NaIO_3$ (33 mg/kg). Retinas were imaged one week later. Arrowheads indicate areas of retinal degeneration. (B) Fundus photographs were converted to greyscale and thresholded to identify the percentage area with significant degeneration (white) as a percent of the entire field (black). (C) $NaIO_3$ challenge induced significant retinal degeneration in control mice pre-treated by two days, one week, and two weeks. For all pre-treatment periods, only crySI significantly reduced the area of retinal degeneration. Data are presented as mean ± SD (n = 6–10, *$p < 0.05$, ****$p < 0.0001$). (D) For animals pre-treated two days prior to $NaIO_3$, H&E histopathology is presented to visualize retinal cryo-sections post-challenge. The epithelial monolayer was entirely disrupted and RPE cells showed a rounded, degenerative phenotype (see arrows) in all groups, except in the crySI pre-treated retinas. Predominant

loss of RPE cells, distortion and thinning of the ONL and disorganization of the INL were also observed. Pre-treatment with crySI preserved retinal layers including RPE and photoreceptors (see arrows). GCL = Ganglion cell layer; INL = Inner nuclear layer; ONL = Outer nuclear layer; RPE = Retinal pigment epithelium; CHO = Choroid. Scale bar: 50 μm.

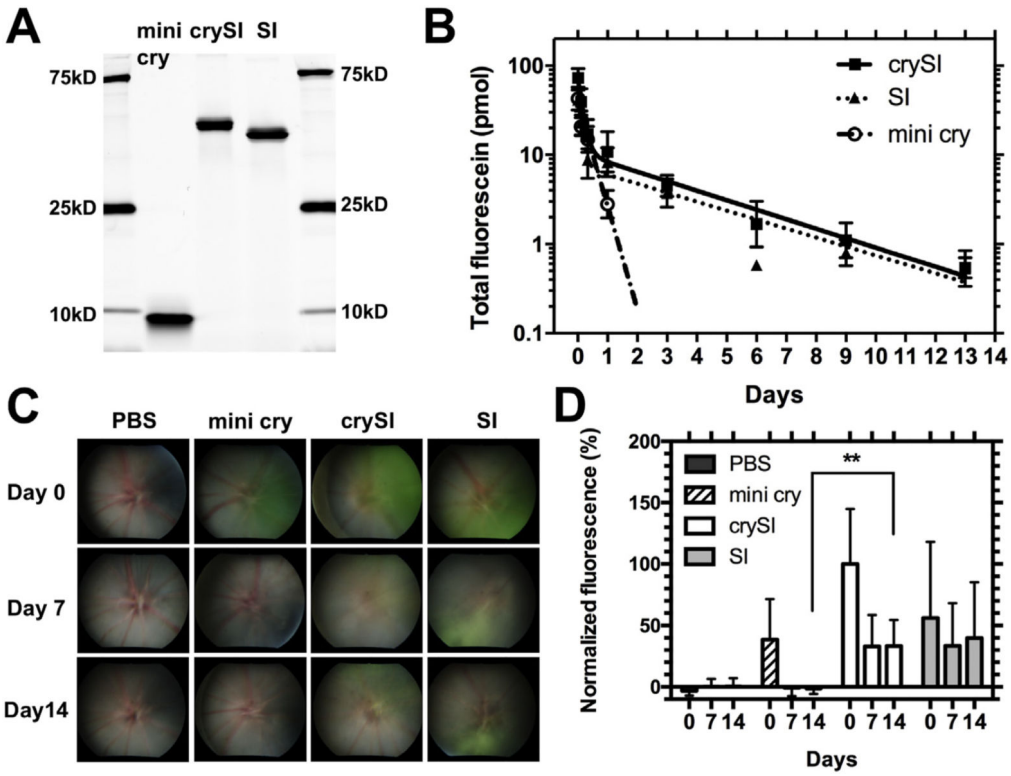

Fig. 3.

Intra-vitreal crySI is retained for long durations near the retina. (A) SDS-PAGE shows the identity and purity of fluorescently labeled mini cry, crySI, and SI along with a molecular weight marker. While the fluorescein labeled mini cry peptide electrophoreses at a higher molecular weight than expected; its exact mass (2.78 kD) was confirmed independently by electrospray mass spectrometry. (B) The total amount of dye-labeled mini cry, crySI and SI in the mouse eye was quantified over a 2-week window post intra-vitreal administration. Data for mini cry (0–1 day) were fit by a single exponential decay due to its fast clearance within 3 days. Data for crySI and SI (0–13 days) were fit to a bi-exponential decay (Eq. (4)). Fusion to the ELP improves the ocular pharmacokinetics compared to mini cry. Data are expressed as mean ± SD (n = 4). (C) The retention of mini cry, crySI and SI was monitored by fundus photography following intra-vitreal injection. The appearance of signal (green) in representative fundus images demonstrates the prolonged ocular retention of crySI. (D) The normalized fluorescence (Eq. (3)) was plotted for indicated time points. CrySI exhibited longer ocular retention with significantly more signal remaining than mini cry after two weeks. Data are expressed as mean ± SD (n = 3–5, **$p < 0.01$).(For interpretation of the references to color in this figure legend, the reader is referred to

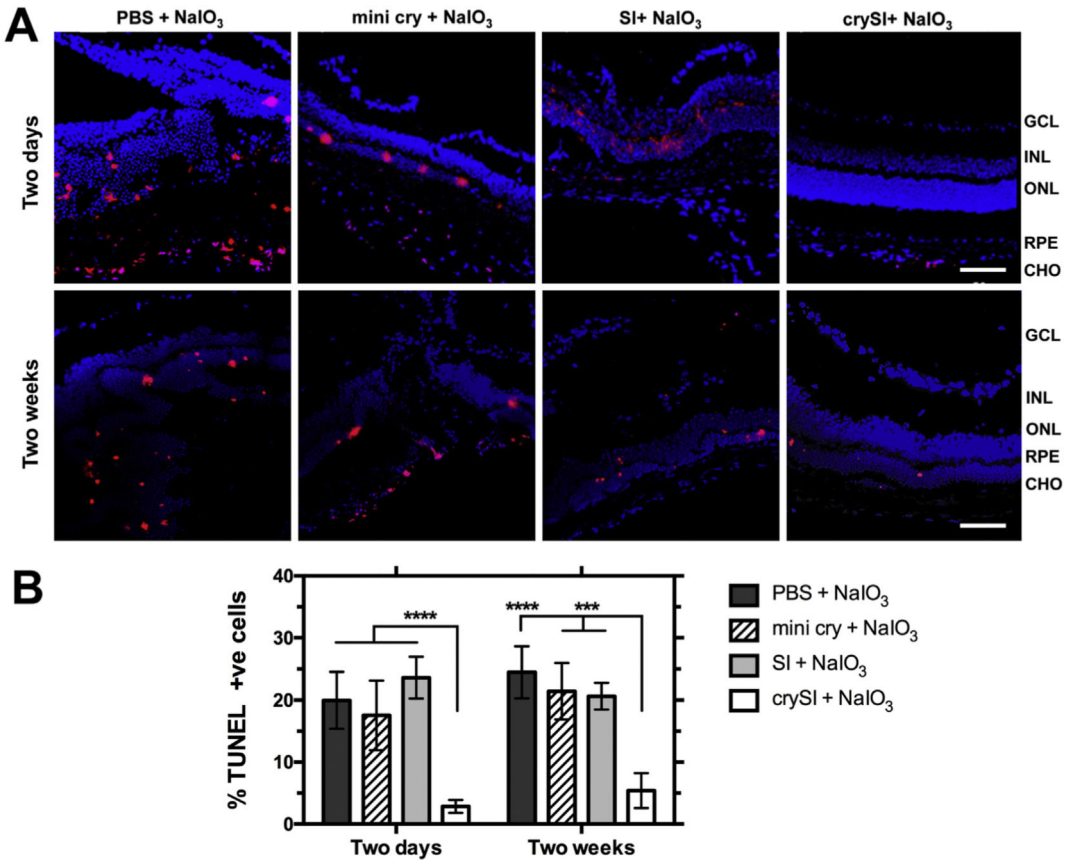

Fig. 4.

Intra-vitreal crySI protects against NaIO3-induced apoptosis in the retina. *129S6/SvEvTac* mice were pre-treated with PBS, mini cry, SI, and crySI two days or two weeks prior to $NaIO_3$ challenge. (A) TUNEL-positive cells (red) were detected in cryo-sections from the retina. Apoptotic cells are observed in the ONL, RPE, and choroid. Scale bar: 50 μm. (B) Quantification revealed that the percentage of TUNEL positive cells in the crySI group was significantly decreased after $NaIO_3$ treatment when compared to other groups. Data are shown as mean ± SD (n=4–7, ****$p < 0.0001$, ***$p < 0.001$). (For interpretation of the references to color in this figure legend, the reader is referred to the web version of this article.)

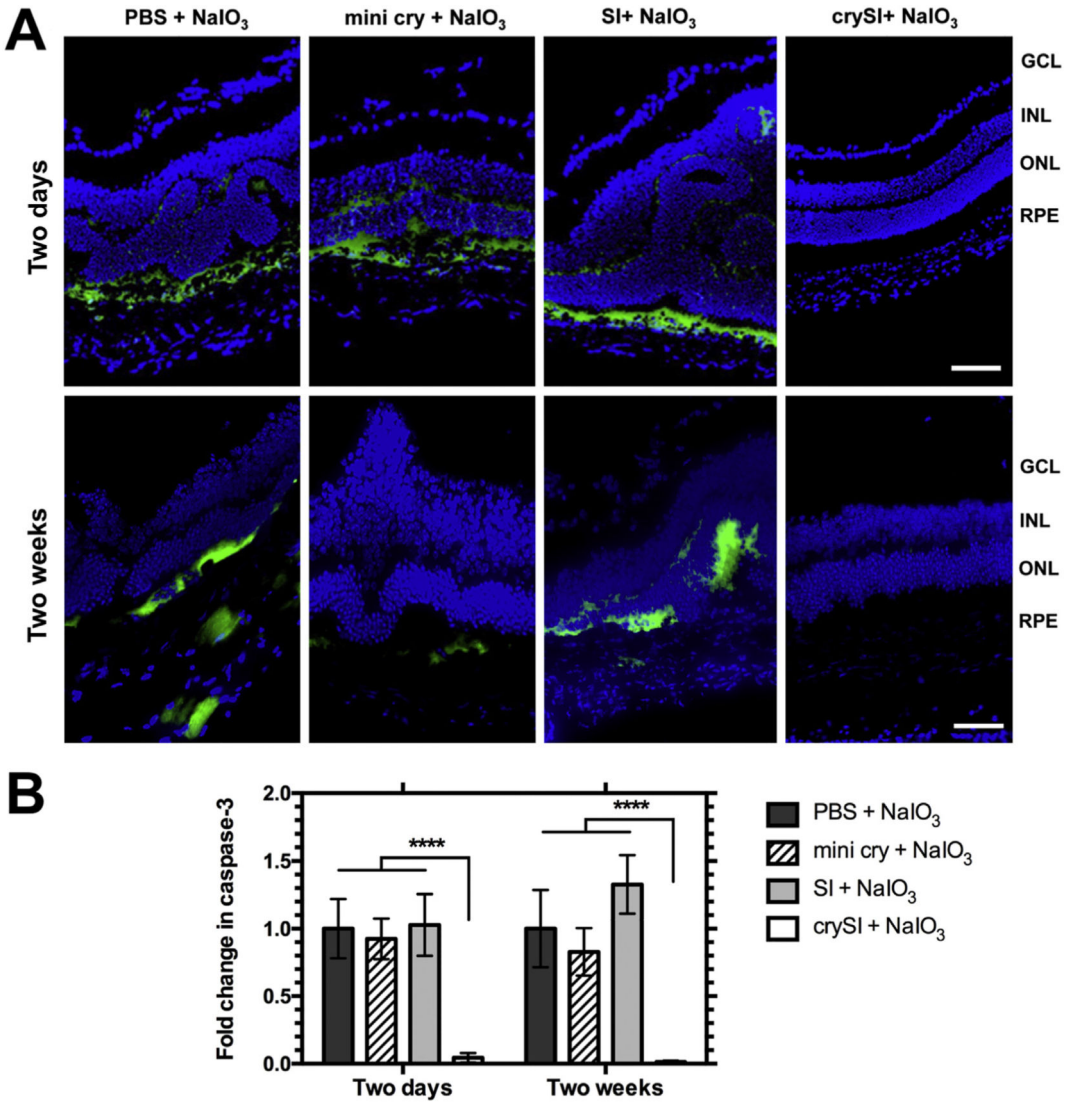

Fig. 5.

Intra-vitreal crySI prevents $NaIO_3$-induced cell death through caspase-3 regulation. *129S6/SvEvTac* mice were pre-treated with PBS, mini cry, SI and crySI two days or two weeks prior to $NaIO_3$ challenge. (A) Secondary immunofluorescence was used to detect cleaved Caspase-3 (Casp3) in cryo-sections of the retina. Caspase-3 activation was inhibited in crySI treated mice when compared to PBS, SI, or mini cry treated groups. Scale bar: 50 μm. (B) Quantification revealed that in the crySI groups, caspase-3 activation was significantly lower than in other groups. Data are shown as mean ± SD (n=5–7, ****$p < 0.0001$).

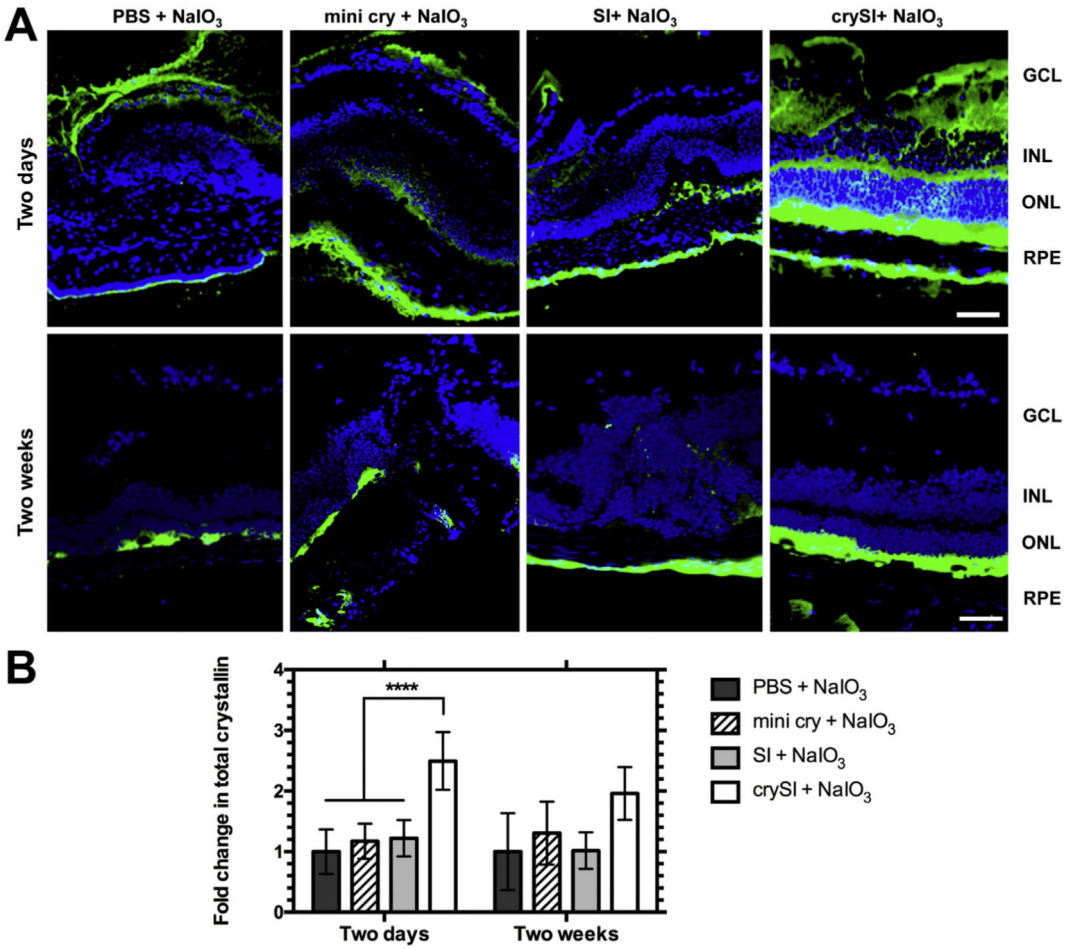

Fig. 6.

Intra-vitreal crySI enhances the accumulation of αB crystallin. *129S6/SvEvTac* mice were pre-treated with PBS, mini cry, SI and crySI two days or two weeks prior to $NaIO_3$ challenge. (A) Secondary immunofluorescence was used to detect both endogenous αB crystallin and residual exogenous crySI in cryo-sections of the retina. Due to antibody cross-reactivity, CrySI enhanced the staining for total αB crystallin detected in the RPE, INL, ONL layers in the two day pre-treatment groups (obtained 9 days after treatment with CrySI). In contrast, the two week pre-treatment retinas (obtained 6 weeks after treatment with CrySI) revealed a level and pattern of staining consistent with endogenous αB crystallin. Scale bar: 50 μm. (B) Quantification revealed that total crystallin level was significantly increased in the two-day pretreated crySI group compared to other controls. Data are shown as mean ± SD (n=5–7, ****$p < 0.0001$).

Table 1

Nomenclature, sequence, molecular weight and purity of mini cry and ELP fusion proteins.

Peptide label	Amino acid Sequence	M.W. [kD]	Purity [%]
mini cry	DRFSVNLDVKHFSPEELKVK	2.4*	98.1***
SI	$G(VPGSG)_{48}(VPGIG)_{48}Y$	39.7**	99.2****
crySI	$GDRFSVNLDVKHFSPEELKVKG(VPGSG)_{48}(VPGIG)_{48}Y$	42.1**	88.3****

* Chemically synthesized from amino acids 73–92 of the human αB crystallin protein.

** Expected M.W. based on the open reading frame, excluding a methionine start codon.

*** Purity estimated from RP-HPLC.

**** Purity estimated from SDS-PAGE.

Table 2

Ocular pharmacokinetics of mini cry and ELPs following intra-vitreal administration to mice.

Parameter	Unit	Mini cry* (n=4)		crySI** (n=4)		SI** (n=4)	
		Mean	[95% CI]	Mean	[95% CI]	Mean	[95% CI]
X_0	[pmol]	38.5	[29.7 to 47.3]	76.0	[49.6 to 102.5]	45.1	[27.1 to 63.0]
f_{fast}		1	na	0.86	[0.79 to 0.93]	0.83	[0.74 to 0.93]
k_{fast}	[day^{-1}]	2.7	[2.2 to 3.1]	6.6	[2.7 to 10.6]	8.5	[1.9 to 15.1]
k_{slow}	[day^{-1}]	na	na	0.24	[0.19 to 0.30]	0.23	[0.17 to 0.29]
$t_{half,\ fast}$	[days]	0.26	[0.22 to 0.32]	0.10	[0.07 to 0.26]	0.08	[0.05 to 0.37]
$t_{half,\ slow}$	[days]	na	na	2.8	[2.3 to 3.7]	3.0	[2.4 to 4.0]
AUC***	[pmol days]	14.5	na	56.2	na	38.4	na
AUMC***	[pmol days^2]	6.2	na	169.0	na	130.5	na
MRT***	days	0.4	na	3.0	na	3.4	na

na: not applicable.

* mini cry data (0–1 day) were fit to a mono-exponential decay equation.

** crySI and SI data (0–13 days) were fit to a bi-exponential decay equation.

*** AUC, AUMC, and MRT were estimated using a non-compartmental method.